Environ Geol (2009) 56:1145–1159
DOI 10.1007/s00254-008-1215-2

ORIGINAL ARTICLE

Analysis of rainfall-induced infinite slope failure during typhoon using a hydrological–geotechnical model

Agus Setyo Muntohar · Hung-Jiun Liao

Received: 1 September 2007 / Accepted: 22 January 2008 / Published online: 7 February 2008

Abstract Rainwater infiltration during typhoons tends to trigger slope instability. This paper presents the results of a study on slope response to rainwater infiltration during heavy rainfall in a mountain area of Taiwan. The Green-Ampt infiltration model is adopted here to study the behavior of rainwater infiltration on slopes. The failure mechanism of infinite slope is chosen to represent the rainfall-induced shallow slope failure. By combining rain infiltration model and infinite slope analysis, the proposed model can estimate the occurrence time of a slope failure. In general, if a slope failure is to happen on a slope covered with low permeability soil, failure tends to happen after the occurrence of the maximum rainfall intensity. In contrast, slope failure tends to occur prior to the occurrence of maximum rainfall intensity if a slope is covered with high-permeability soil. To predict the potential and timing of a landslide, a method is proposed here based on the normalized rainfall intensity (NRI) and normalized accumulated rainfall (NAR). If the actual NAR is higher than the NAR calculated by the proposed method, slope failure is very likely to happen. Otherwise, the slope is unlikely to fail. The applicability of the proposed model to occurrence time and the NAR–NRI relationship is evaluated using landslide cases obtained from the literature. The results of the proposed method are close to that of the selected cases. It verifies the applicability of the proposed method to slopes in different areas of the world.

Keywords Shallow slope failure · Rain infiltration · Green-Ampt model · Infinite slope · Typhoon · Occurrence time of landslide · Rainfall intensity · Accumulated rainfall

List of symbols

c'	effective soil cohesion (kPa)
$F(t)$	cumulative infiltration at time t (mm)
$f(t)$	infiltration rate at time t (mm/h)
$F'(t)$	tentative cumulative infiltration at time t (mm)
$f'(t)$	tentative infiltration rate at time t (mm/h)
$I(t)$	rainfall intensity at time t (mm/h)
k	coefficient of hydraulic conductivity (mm/h)
k_{sat}	coefficient of saturated hydraulic conductivity (mm/h)
NAR	normalized accumulated rainfall (mm^{-1} h)
NRI	normalized rainfall intensity (mm^{-1})
$R(t)$	accumulated rainfall at time t (mm)
t	elapsed time (h)
T_f	critical time of failure (h)
T_p	time at maximum rainfall intensity (h)
t_p	ponding time (h)
u_a	pore air pressure (kPa)
u_w	pore water pressure (kPa)
z_w	depth of wetting front (mm)
Δt	time interval (h)
ΔT	time interval of rolling rainfall (h)

A. S. Muntohar
Department of Civil Engineering,
Universitas Muhammadiyah Yogyakarta,
D.I. Yogyakarta, Indonesia
e-mail: muntohar@umy.ac.id

H.-J. Liao
Department of Construction Engineering,
National Taiwan University of Science and Technology,
Taipei, Taiwan

H.-J. Liao (✉)
No. 43, Section 4, Keelung Road, Taipei 10699, Taiwan
e-mail: hjliao@mail.ntust.edu.tw

$\Delta\theta$	deficit of the volumetric moisture content ($mm^3\ mm^{-3}$)
β	topographical slope angle
ϕ'	effective friction angle
ϕ^b	friction angle linked to matric suction, $u_a - u_w$
γ_t	unit weight of soil (kN m^{-3})
γ_w	unit weight of water = 9.81 kN m^{-3}
η	the soil porosity
θ	volumetric moisture content ($mm^3\ mm^{-3}$)
θ_e	effective porosity
θ_i	initial moisture content
θ_s	volumetric moisture content at saturation
σ_n	normal stress (kPa)
τ_n	shear stress parallel to failure plane (kPa)
ψ_f	suction head at wetting front (L)

Introduction

A landslide is a natural soil movement. But it also poses a threat to the human life and the property. Of the 52 typhoons, which attacked Taiwan between 1994 and 2004, each caused many landslide problems along mountain roads. Landslides caused by these typhoons are classified into three major categories: (1) soil or rock fall, (2) debris flow, and (3) earth slide. Among them, the earth sliding type failure in the form of shallow slope failure and limited amount of moving debris is the dominant failure type (Liao et al. 2006).

A great deal of research has been carried out on the failure mechanism and failure probability of rainfall induced landslides. Typically, the rainfall data being input to landslide study includes only the rainfall intensity and the accumulated rainfall of a rainfall event. Very little effort has been made to establish the relationship among rainfall, rain infiltration to the ground, and slope stability. So, this paper will focus on the response of slopes to the infiltration of rainwater. To quantify the effect of rainfall on the stability of a slope, a critical rainfall infiltration index will be introduced in this paper.

For both the empirical and physical methods adopted to study rainfall-induced landslides, the occurrence time of a landslide is commonly estimated based on the rainfall intensity and/or the accumulated rainfall. So far, several empirical equations and graphs have been developed to study rainfall-induced landslides. Among the parameters studied, critical rainfall and its duration time are the most commonly used. However, the empirical graphs or equations vary from one to another. Their application is limited to certain specific areas. In contrast, the physical method requires more detailed slope information such as: shear strength parameters, rainfall data, pore water, data and water content records. But, these parameters are not readily available. Field measurement is generally required to gather parameters needed for the physical method.

The main objective of the research is to look into the change of slope stability in response to rainwater infiltration. Subjects studied here include (1) estimating the occurrence time of landslide, and (2) establishing relationships among the rainfall data, rainwater infiltration, slope hydraulic properties, and slope stability. The latter will be used to generate the value of critical rainfall, which will predict the occurrence of a landslide. By combining the rain infiltration model and the infinite slope stability analysis (hydrological–geotechnical model), a model for analyzing rainfall-induced landslides is proposed here.

Infiltration model

The commonly used Green-Ampt model for one-dimensional rainwater infiltration is adopted here. Relatively, the Green-Ampt model is a simple infiltration model. But, it can generate results, which are in good agreement with rigorous models such as Richard's equation (Claunitzer et al. 1998; Hsu et al. 2002). Originally, this model was developed for ponding water infiltration on horizontal surfaces. Hence, in its application to sloping ground surface, it needs modification. Following are the modified Green-Ampt equations for sloping ground surface proposed by Chen and Young (2006):

$$f(t) = k\left[\cos\beta + \frac{(\psi_f \cdot \Delta\theta)}{F(t)}\right] \tag{1}$$

$$F(t) - \frac{(\psi_f \cdot \Delta\theta)}{\cos\beta}\ln\left[1 + \frac{F(t)\cos\beta}{(\psi_f \cdot \Delta\theta)}\right] = k_y \cdot t \tag{2}$$

where $f(t)$ = potential infiltration rate at time t, $F(t)$ = cumulative infiltration at time t, ψ_f = suction head at wetting front, $\Delta\theta$ = volumetric water content deficit (= $\theta_s - \theta_i$), β = slope angle (for horizontal surface $\beta = 0$), $k_y = k\cos\beta$, and k = coefficient of hydraulic conductivity. In this study, the parameters $\Delta\theta$ and ψ_f are combined as one parameter and called the moisture-suction ($\psi_f\Delta\theta$). The hydraulic conductivity and moisture-suction are the inherent parameters of soil. They can be obtained from the laboratory or field tests. Table 1 summarizes the range of Green-Ampt parameters for various soil types (USDA classifications) (Chow et al. 1988).

The Green-Ampt infiltration model is assumed to meet the following conditions:

1. the suction head at wetting front is constant,
2. the deficit of volumetric water content is uniform before and after wetting (see Fig. 1),
3. the coefficient of hydraulic conductivity is constant and equal to saturated hydraulic conductivity (k_{sat}).

Table 1 Parameters needed in Green-Ampt infiltration model (adapted from Chow et al. 1988)

Soil type	Range of η	Range of θ_e	Range of ψ_f (mm)	k (mm/h)	ψ_f (mm)	$k_s = 2k$[a] (mm/h)
Sand	0.374 ~ 0.5	0.354 ~ 0.48	9.7 ~ 253.6	117.8	49.5	235.6
Loamy sand	0.363 ~ 0.506	0.329 ~ 0.473	13.5 ~ 279.4	29.9	61.3	59.8
Sandy loam	0.351 ~ 0.555	0.283 ~ 0.541	26.7 ~ 454.7	10.9	110.1	21.8
Loam	0.375 ~ 0.551	0.334 ~ 0.534	13.3 ~ 593.8	3.4	88.9	6.8
Silt loam	0.42 ~ 0.582	0.394 ~ 0.578	29.2 ~ 953.9	6.5	466.8	13
Sandy clay loam	0.332 ~ 0.464	0.235 ~ 0.425	44.2 ~ 1,080	1.5	218.5	3
Clay loam	0.409 ~ 0.519	0.279 ~ 0.501	47.9 ~ 911	1	208.8	2
Silty clay loam	0.418 ~ 0.524	0.347 ~ 0.517	56.7 ~ 1,315	1	273	2
Sandy clay	0.37 ~ 0.49	0.207 ~ 0.435	40.8 ~ 1,402	0.6	239	1.2
Silty clay	0.425 ~ 0.533	0.334 ~ 0.512	61.3 ~ 1,394	0.5	292.2	1
Clay	0.427 ~ 0.523	0.269 ~ 0.501	63.9 ~ 1,565	0.3	316.3	0.6

[a] Rawls et al. 1993

The soil studied in the Green-Ampt model is assumed to be fully saturated from the surface to the depth of wetting front during infiltration, but the soil below the wetting front still remains its initial degree of saturation. The vertical depth of wetting front can be estimated by the following equation:

$$z_w = \frac{F(t)}{(\theta_s - \theta_i)\cos\beta} \tag{3}$$

The Green-Ampt model can be applied to both steady state rainfall intensity and unsteady state rainfall intensity. But only the latter is investigated in this study. During a rainfall event, the potential infiltration rate calculated from the Green-Ampt equation can result in three possible cases as shown in Fig. 2: (1) Rainfall intensity is larger than potential infiltration rate. Ground surface is in saturated state in this time interval (case 1); (2) Rainfall intensity is smaller than the potential infiltration rate at the beginning of the time interval but becomes larger than the potential infiltration rate later. So the ground surface changes from unsaturated to saturated in this time interval (case 2); (3) Rainfall intensity is smaller than infiltration rate. There is no surface saturation in this time interval (case 3). For case 3, all the rainfall infiltrates into soil. But the surface is not saturated. The surface saturation occurs only if the potential infiltration rate becomes less than the rainfall intensity. Hence, the infiltrated rainfall can be calculated using the following equation:

$$F(t+\Delta t) - F(t) - \frac{(\psi_f \cdot \Delta\theta)}{\cos\beta} \cdot \ln\left[\frac{(F(t+\Delta t)\cos\beta + \psi_f \cdot \Delta\theta)}{(F(t)\cos\beta + \psi_f \cdot \Delta\theta)}\right] = k_y \cdot \Delta t \tag{4}$$

Beyond this time, any additional rainfall will become surface run-off.

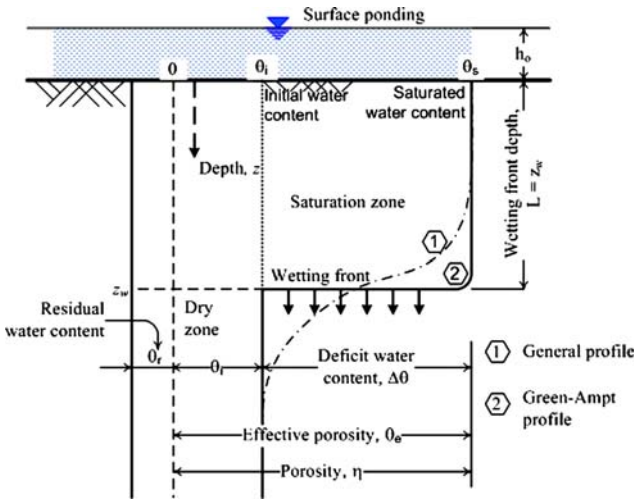

Fig. 1 Infiltration profile for Green-Ampt model

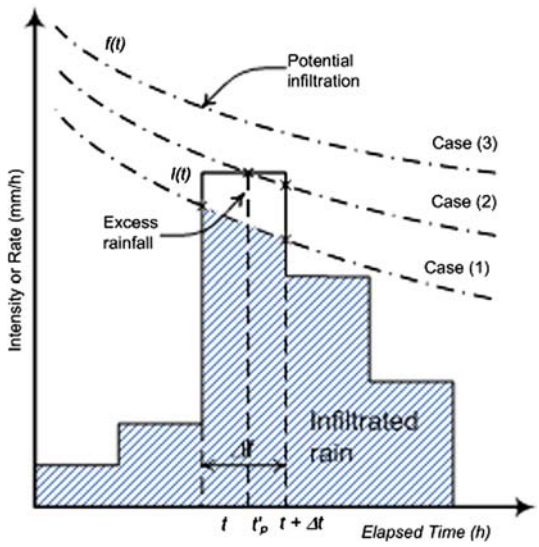

Fig. 2 Rainwater infiltration and rainfall intensity in Green-Ampt model

If case 2 occurs, the infiltrated rainfall can be calculated using the following equation:

$$F\left(t'_{\mathrm{p}}\right) = \frac{k_{\mathrm{sat}} \cdot (\psi_{\mathrm{f}} \cdot \Delta\theta)}{I(t) - k_{\mathrm{sat}} \cos\beta} \tag{5}$$

The time needed to reach saturation is defined as follows:

$$t'_{\mathrm{p}} = \frac{F\left(t'_{\mathrm{p}}\right) - F(t)}{I(t)} \tag{6}$$

Slope stability model

When raining, rainwater infiltrates into the subsurface soil through the unsaturated zone on the top. This process results in a wetted zone at shallow depth near the slope surface and may lead to slope failure during a prolonged or heavy rainfall period. This type of slope failure usually occurs in the form of sliding or shallow slip parallel to the slope surface. So it is analyzed using the infinite slope model here in this study (Fig. 3). Considering the unsaturated soil behavior, the factor of safety against an infinite slope sliding is estimated using the Mohr–Coulomb failure criterion (Fredlund et al. 1978):

$$\mathrm{FS} = \frac{c' + (\sigma_{\mathrm{n}} - u_{\mathrm{a}}) \tan\phi' + (u_{\mathrm{a}} - u_{\mathrm{w}}) \tan\phi^{\mathrm{b}}}{\gamma_{\mathrm{t}} z_{\mathrm{w}} \sin\beta \cos\beta} \tag{7}$$

As shown in Eq. 7, the matric suction $(u_{\mathrm{a}} - u_{\mathrm{w}})$ decreases with increasing water content and becomes 0 when the soil is fully saturated. The value of ϕ^{b} is related to the matric suction; ϕ^{b} is close to the effective friction ϕ' of soil at low suction (Fredlund et al. 1978). In this study, it is assumed that ϕ^{b} is equal to ϕ', u_{a} is the atmospheric pressure and $(u_{\mathrm{a}} - u_{\mathrm{w}}) = -\psi_{\mathrm{f}} \cdot \gamma_{\mathrm{w}}$. The normal stress, $\sigma_n = \gamma_t z_w \cos^2\beta$, then Eq. 7 is rewritten as follows:

$$\begin{aligned}\mathrm{FS} &= \frac{c' + \gamma_{\mathrm{t}} z_{\mathrm{w}} \tan\phi' + \psi_{\mathrm{f}} \cdot \gamma_{\mathrm{w}} \tan\phi'}{\gamma_{\mathrm{t}} z_{\mathrm{w}} \sin\beta \cos\beta} \\ &= \frac{\tan\phi'}{\tan\beta} + \frac{c' + \psi_{\mathrm{f}} \cdot \gamma_{\mathrm{w}} \tan\phi'}{\gamma_{\mathrm{t}} z_{\mathrm{w}} \sin\beta \cos\beta}\end{aligned} \tag{8}$$

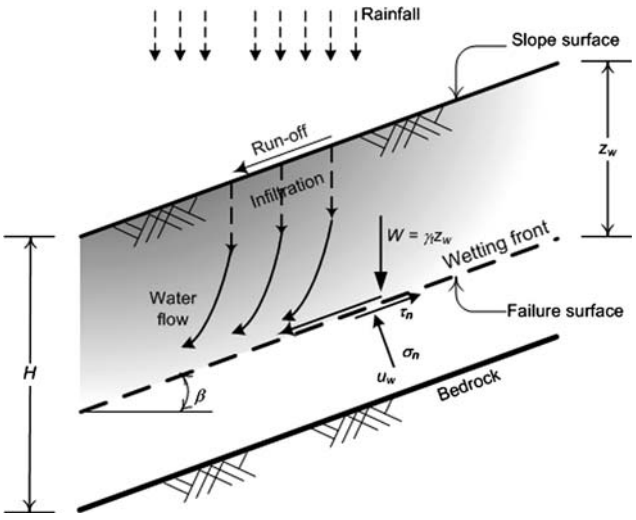

Fig. 3 Infinite slope model to analyze rain infiltration induced shallow failure

Model study

In this study, the slopes along the T18 mountain road in central Taiwan are chosen as the sample cases. The slope angle of the roadside slopes varies from 40° to 80° (average slope angle $\beta = 60°$). According to the previous site investigation (see Fig. 4) performed (Land Engineering Consultant Co. Ltd. 2005), the covering materials on the slope are mainly mixtures of gravel–sand–silt or sand–silt. The thicknesses of covering colluvial soil are equal to 9, 10, and 17 m at boreholes B4, B3, and B1, respectively. Other investigations carried out nearby reported that the colluvial layer was around 5–6 m thick (Chang et. al. 2005).

The porosity of slope covering soil ranges from 0.1 to 0.34 (average soil porosity, $\eta = 0.26$). Based on the particle size distribution and the soil porosity, the suction head of slope covering soil can be estimated using Arya and Paris (1981) method for a soil–water characteristics curve (SWCC). The suction head at wetting front is determined using the air-entry pressure (AEP) head obtained from the SWCC. Based on the SWCC, the AEP varies from 1 to 800 mm. The shear strength parameters were obtained from laboratory tests. Effective cohesion c' ranges from 0 to 50 kPa (average $c' = 22$ kPa) and effective friction angle ϕ' ranges from 17° to 31° (average $\phi' = 20°$). The saturated hydraulic conductivity of slope covering soil is taken to be 36–360 mm/h and 0.36–3.6 mm/h for exposed areas and vegetated areas, respectively. Table 2 summarizes the parameters used in rain infiltration and slope stability analyses.

To study the slope instability caused by rain infiltration induced, rainfall data monitored in the field are used here. The precipitation data used were collected from the rain gauges installed at mileposts 27K + 200, 54K + 200, and 64K + 800 of T18 road. Three typhoons, Ewiniar, Bilis, and Kaemi, which attacked Taiwan in July 2006, were chosen as the rainfall events for the rain infiltration analysis. Figure 5 shows the hourly rainfall intensity and accumulated rainfall for each typhoon recorded at each chosen location. During typhoon Ewiniar, rainfall persisted with moderate intensity for 13 h. Then, 4 h later, intensive rainfall continued for a period of 19 h. During this time

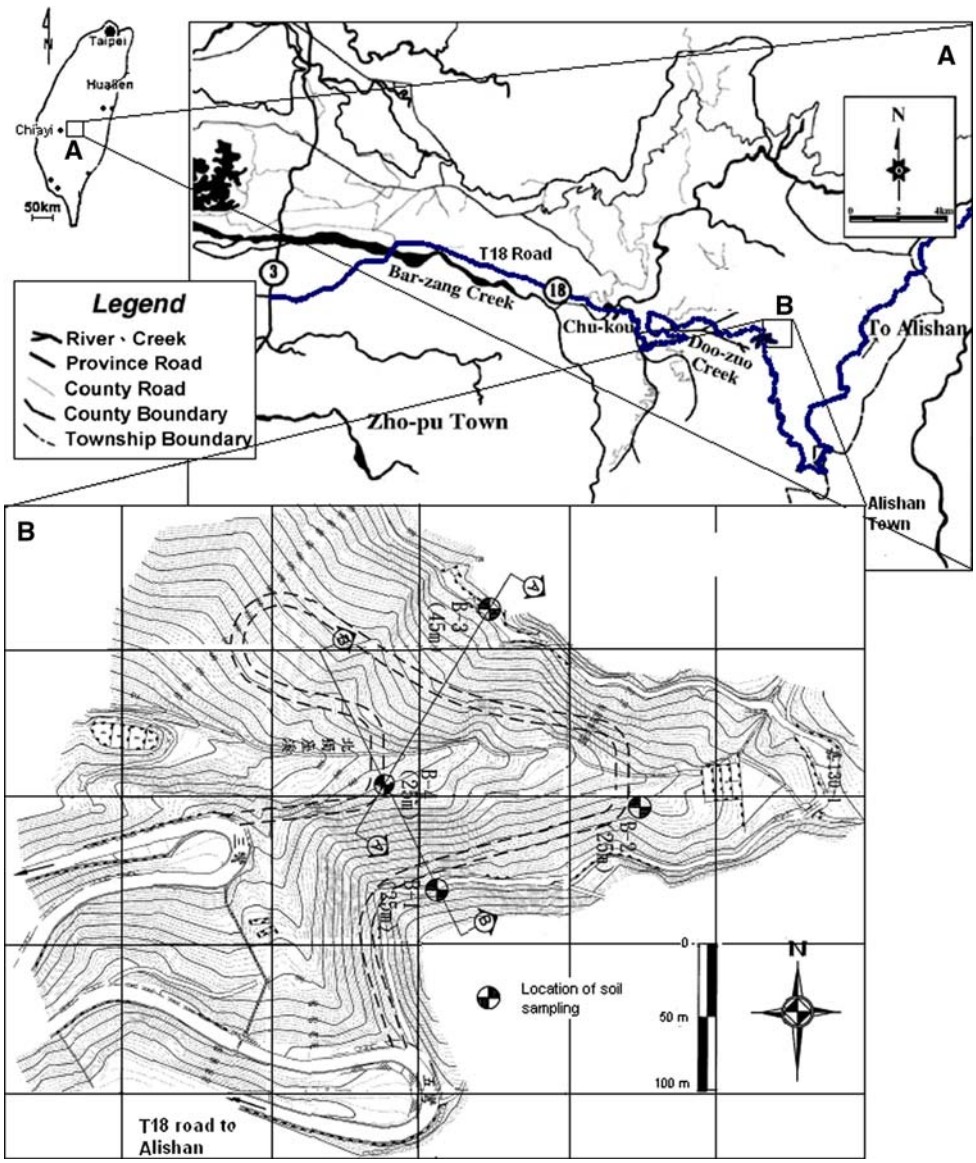

Fig. 4 Soil sampling locations on the T18 mountain road, Central Taiwan (Land Engineering Consultant Co. Ltd. 2005)

Table 2 Green and Ampt parameters and soil shear strength properties used in this study

Parameters	Values
Hydraulic conductivity, k_{sat}^{a}	Soil 1: 360 mm/h; soil 2: 36 mm/h; soil 3: 3.6 mm/h; soil 4: 0.36 mm/h
Initial water content, θ_i	7–18.6 (%) (13.1%)
Water-content deficit, $\Delta\theta$	0.029–0.191 (0.123)
Wetting front suction head, ψ_f	1–800 mm
Soil cohesion, c'	0–50 (22) kPa
Soil friction angle, ϕ'	17°–31° (20°)
Unit weight, γ_t	19.7–24.8 (21.8) kN/m^3

Number in parenthesis is the average value

[a] Degree of permeability from high to low

period, the accumulated rainfall approached 400 mm. The maximum rainfall intensity was 68 mm/h, which was recorded 6–7 h after the pouring rainfall started. Typhoon Bilis brought in a large amount of rainfall with the accumulated rainfall approaching 900 mm between July 14 and 16, 2006 (60 h). The maximum rainfall intensity was 44.5 mm/h, which was recorded about 15–16 h after the rainfall started. Rainfall continued for 24 h during typhoon Kaemi. The accumulated rainfall recorded during this time interval was about 190 mm. The maximum rainfall intensity was recorded 12–13 h after the rainfall started. Subsequently, moderate rainfall intensity continued until typhoon Kaemi left Taiwan. The sequence of rainfall infiltration analysis and slope stability analysis is illustrated

in the flow chart shown in Fig. 6. Based on the study carried out by Chang et al. (2005), the rainfall events before the typhoon (i.e., antecedent rainfall) or heavy rainfall had little effect on the slope instability. This is clear from the lateral deformation observed using the in-situ inclinometer. The deformation data showed an insignificant increment in lateral movement during the antecedent rainfall period. Considering this finding, the effect of antecedent rainfall on the slope stability analysis was ignored in this study.

Results and discussion

Slope response

In this study, the rainfall infiltration and slope stability analysis were calculated using parameters ranging from lower bound to upper bound. For example, the hydraulic conductivity, k_{sat}, of covering soil is the most influential parameter affecting rainfall infiltration induced slope instability (Muntohar and Liao 2007). Hydraulic conductivities, k_{sat} with a range of three orders of magnitude (0.36–360 mm/h) were used as input to study their effects on factor of safety. On the other hand, for soil parameters, which are less influential with regard to slope stability, average values of soil parameters can be used. To demonstrate this parametric study results, Fig. 7 is adopted here as an example. This figure shows the changes of slope stability and wetting front in response to the rainfall recorded during different typhoons. The slope safety factor is computed using the following slope information: $\beta = 60°$, $\psi_f = 800$ mm, $\Delta\theta = 0.123$, $c' = 22$ kPa, $\phi' = 20°$, and $\gamma_t = 21.8$ kN/m^3. In general, the slope stability reduces with increasing depth of wetting front, while the depth of wetting front increases with the elapsed time of rainfall. The rainwater infiltration and stability of a slope are affected by the permeability of soil. Rainwater infiltrates deeper in a slope with higher permeability [in Fig. 7 labeled as [1], $k_{sat} = 360$ mm/h and [2], $k_{sat} = 36$ mm/h]

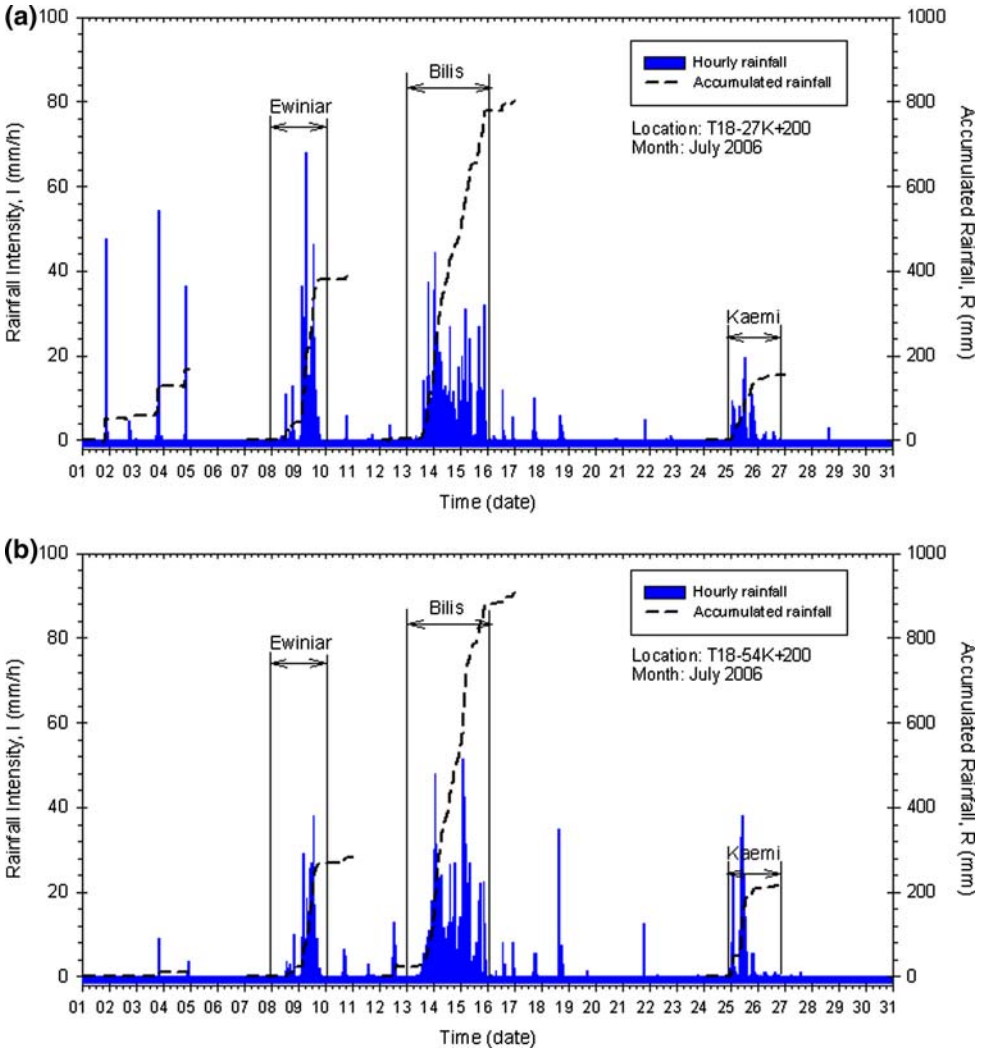

Fig. 5 Rainfall hyetograph recorded in July 2006 at T18 road mileages **a** 27K ± 200, **b** 54K ± 200, and **c** 64K ± 800

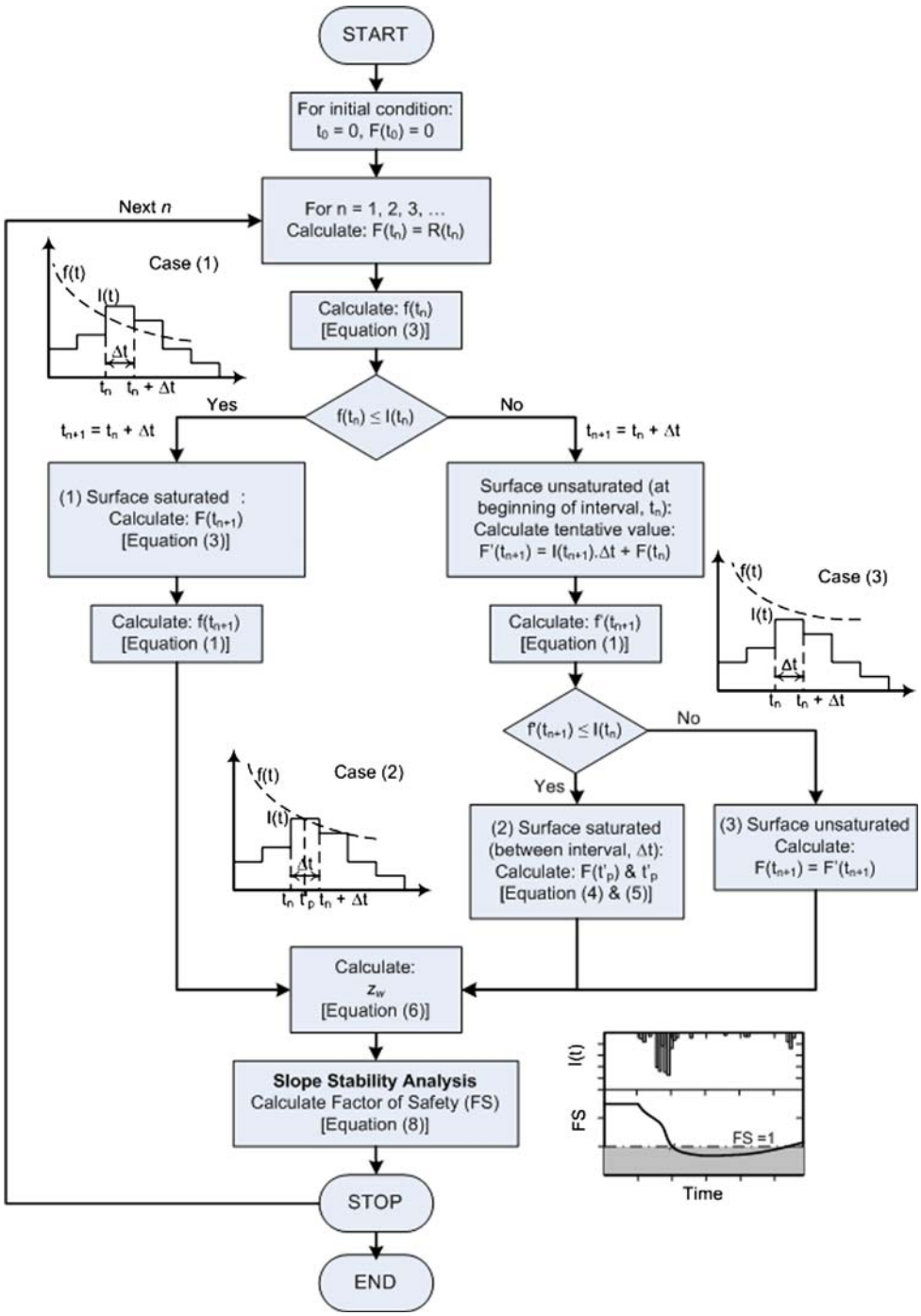

Fig. 6 Slope stability analysis in terms of rain infiltration

but to a shallower depth in a slope with lower permeability [in Fig. 7 labeled as (3), $k_{sat} = 3.6$ mm/h and (4), $k_{sat} = 0.36$ mm/h). It implies that a slope with higher permeability is prone to fail at a deeper depth than a slope with lower permeability. However, for the slopes studied here, only those slopes with higher permeability fail (FS < 1). Slopes with lower permeabilities, such as soil 4, does not fail under the rainfall conditions of these three typhoons. For slopes, which may fail, they tend to fail (FS < 1) when the wetting front reaches a depth of 1.5–3.0 m. As assumed in the model, the failure plane is at the wetting front. So, the failure depth is shallower than the thickness of covering colluvial soil. In other words, its depth is shallower than 5–17 m. Under this condition, it is the infiltration behavior of rainwater that dominates the slope stability rather than the geological features underlying the colluvial soil.

In addition, Fig. 7 also shows the occurrence time of slope failures. The figures show obviously that slopes with

high permeability tend to slide before the time of maximum rainfall intensity occurs. But slopes with low permeability have a tendency to slide after the occurrence time of maximum rainfall intensity. Intense rainfall will infiltrate faster and reach a deeper saturation depth on a slope with high permeability. In contrast, for slopes with low permeability, the rainwater infiltration is slow and the saturation depth is shallow. To reach the instability state, a slope with lower permeability needs more intense rainfall and longer infiltration time to trigger a landslide. Figure 7a, b illustrates that the amount of rolling rainfall in a time period (ΔT) is likely to trigger slope failure. So far, if the starting time of the intense rainfall is known, the occurrence time of landslide (T_f) can be estimated. Based on the results shown in Fig. 7, it can be clearly observed that the failure time of slope varies from 6 to 26 h. But, the failure time of slope determined with the model proposed here varies over a wide range from 6 to 75 h.

During typhoon Ewiniar (Fig. 7a), the slope with higher permeability tends to slide after 5.65–5.89 h of rolling rainfall. During this short time interval, the factor of safety decreases to 1 (FS = 1) and subsequently below 1. At this moment, the amount of rainfall is approaching 165–181 mm. A similar phenomenon was also observed during typhoon Bilis (Fig. 7b). The factor of safety reduced to 1 after 13.6 h of intense rainfall for slopes with high permeability. In other words, the time of landslide occurs 3 h prior to the occurrence of maximum rainfall intensity. During the period of rolling rainfall, the amount of accumulated rainfall is about 160 mm. For a slope with lower permeability (soil 3, k_{sat} = 3.6 mm/h), it tends to fail after 28 h of intense rainfall or 12 h after the occurrence time of

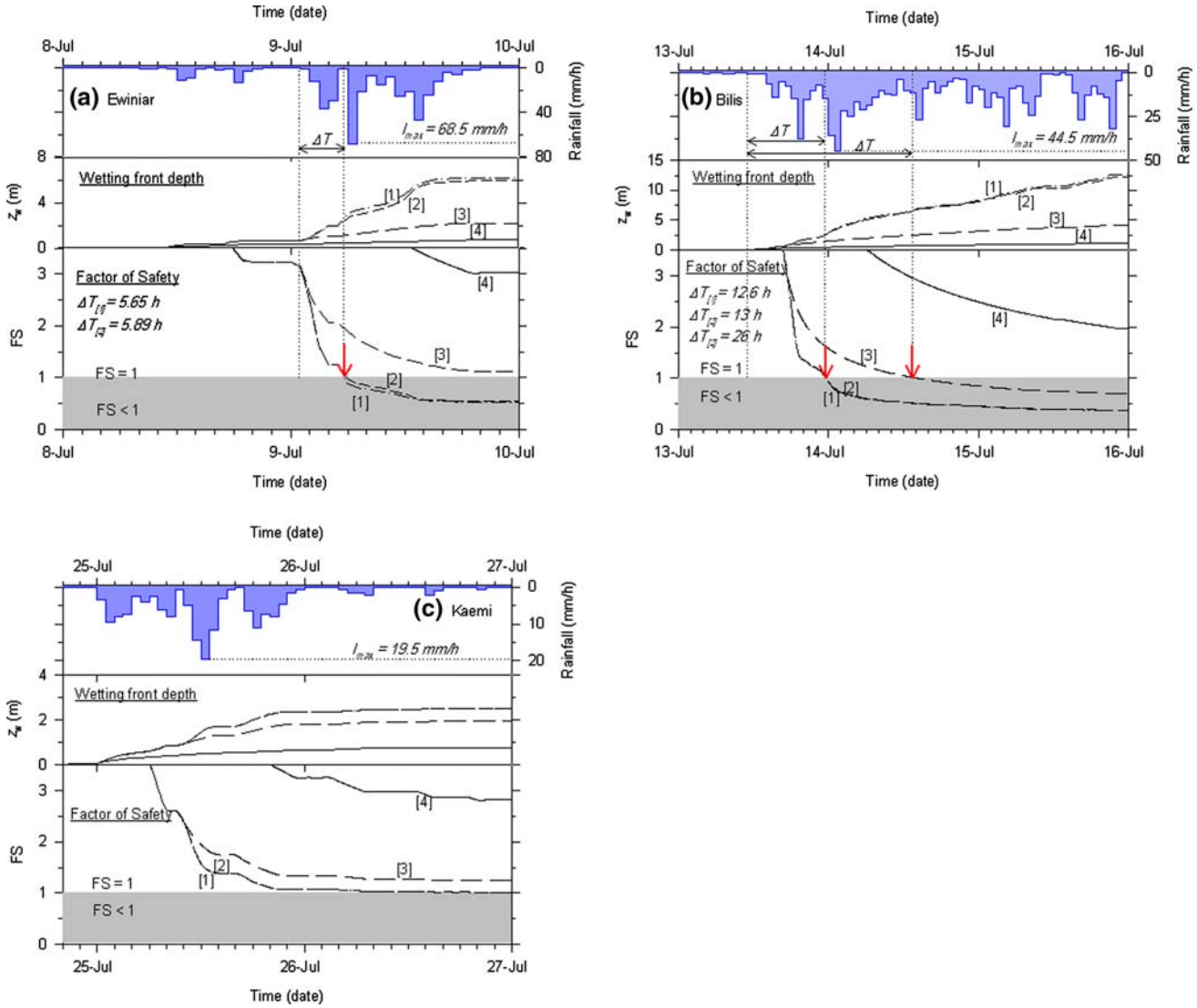

Fig. 7 Slope response during typhoons **a** Ewiniar **b** Bilis **c** Kaemi, for slope with $\beta = 60°$, $\Delta\theta = 0.123$, $\psi_f = 800$ mm, $c' = 22$ kPa, and $\phi' = 20°$ (k_{sat} of soil 1 = 360, soil 2 = 36, soil 3 = 3.6, and soil 4 = 0.36 mm/h)

maximum rainfall intensity. The accumulated rainfall during the period of rolling rainfall is about 427.5 mm. But it should be noted that this slope did not fail during the preceding typhoon, Ewiniar. The accumulated rainfall during typhoon Ewiniar was lower than 400 mm. Hence, a slope with lower permeability is unlikely to fail. But, in Fig. 7a, the factor of safety of the slope labeled [3] approaches FS = 1 at the end of the typhoon. It indicates that a slope with lower permeability needs prolonged intense rainfall and longer infiltration time to trigger a slope failure. During typhoon Kaemi, the slopes did not fail. But, the factor of safety for slope 1 and 2 was approaching FS = 1 when the typhoon ceased. During typhoon Kaemi, the accumulated rainfall was about 150 mm with mean rainfall intensity of 2.9 mm/h. Compared with the two previous typhoons, a slope with high permeability was likely to fail if the amount of rainfall is greater than 160 mm (Bilis), 165–181 mm (Ewiniar). But the amount of rainfall during typhoon Kaemi was not large enough to trigger slope failure; the amount of rainfall was lower than that in previous typhoons (Ewiniar and Bilis). If the rainfall events happened subsequent to the rolling rainfall, the accumulated rainfall would increase and result in a factor of safety less than one. At this state, the slope was very likely to fail.

The amount of landslide triggering rainfall is rather site-dependent and tends to vary from location to location. Chen et al. (2005a) proposed that landslides occur if the accumulated rainfall is over 200 mm and the rainfall intensity is over 20 mm/h based on the landslides monitored in Taiwan. However, this threshold of rainfall does not consider the hydraulic and mechanical properties of slopes. The effect of threshold rainfall is discussed in the following section.

Threshold rainfall

In the limit equilibrium analysis, a slope fails when the driving force is greater than the resisting force (FS < 1). A slope is in critical state when the driving forces are close to the resisting forces (FS ~ 1). According to the results shown in Fig. 7, the response of slope stability to rainfall can be classified into two categories: (1) the slope is in stable state throughout the rainfall period as shown in Fig. 7c, and (2) the slope is stable at the beginning of rainfall and then fails some time later as shown in Fig. 7a, b.

Figure 8 gives an in-depth study on the relationship between rainfall and landslide potential. In Fig. 8, a slope tends to fail when factor of safety decreases to less than 1 (FS < 1). When FS = 1, it indicates that the slope is in the critical state between failed and not failed. So, the time which corresponds to FS = 1 can be defined as the critical time of slope failure (T_f). Starting from T_f, the characteristic of the rainfall event, which will or will not cause slope failure is distinguished quite obviously. The rainfall intensity and accumulated rainfall at this time T_f can be defined as critical rainfall intensity (I_c) and critical accumulated rainfall (R_c). The rainfall, which occurs before the critical rainfall is considered as the triggering rainfall for a landslide. If the triggering rainfall continues to beyond the critical time, then the slope will fail (failed-slope case).

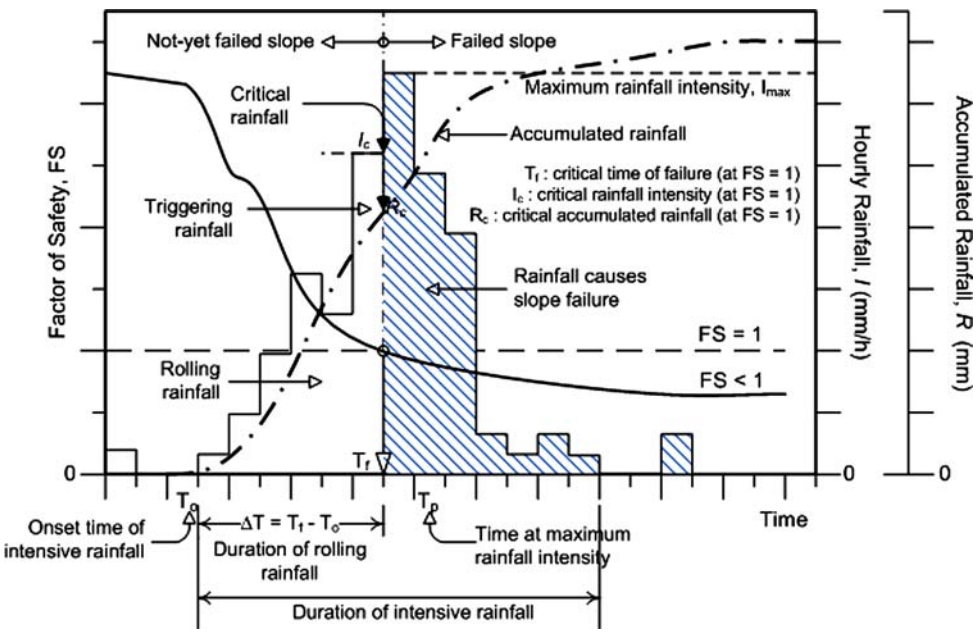

Fig. 8 Typical characteristics of rainfall-induced landslide

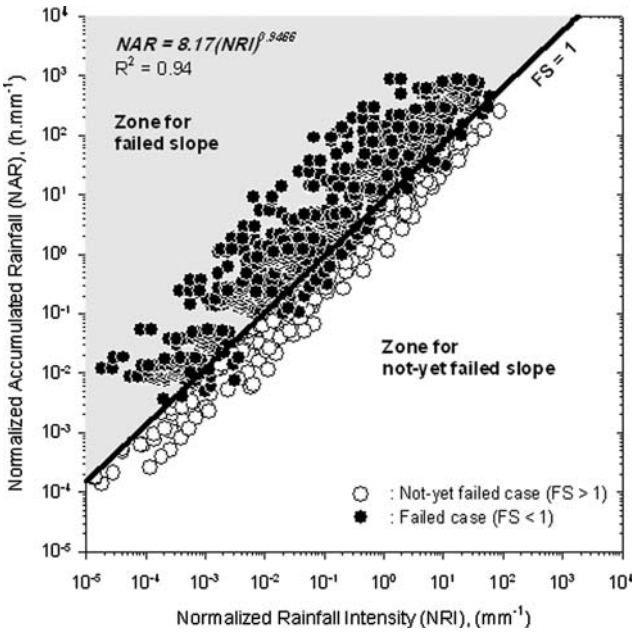

Fig. 9 **a** Rainwater infiltration (note: At crest area, entire rainfall infiltrates into the subsurface. Hence, the infiltration rate is not displayed in the figure), **b** Depth of wetting front, and **c** Factor of safety for the Tenliao slope during typhoon Xangsane

Slope stability is not only affected by rainfall but is also affected by hydraulic properties and physical–mechanical properties of slope material. So, these parameters should be taken into account to establish the relationship between rainfall event and landslide. The proposed relationship is expressed in terms of normalized accumulated rainfall (NAR) and normalized rainfall intensity (NRI). NAR and NRI are defined as

$$\mathrm{NAR} = \frac{R(t)}{(k_{\mathrm{sat}} \cdot \cos\beta \cdot \psi_{\mathrm{f}} \Delta\theta)}$$
$$\mathrm{NRI} = \frac{I(t)}{(k_{\mathrm{sat}} \cdot \cos\beta \cdot \psi_{\mathrm{f}} \Delta\theta)} \quad (9)$$

where $R(t)$ and $I(t)$ is the accumulated rainfall and rainfall intensity at a time t. The units of NAR and NRI are in mm^{-1} h and mm^{-1}, respectively. Figure 9 shows the not-yet failed, and failed slope cases plotted on NAE and NRI charts.

The points plotted in Fig. 9 are calculated using the slope parameters given in Table 2. The line drawn in Fig. 9 is the best-fitted line, which is expressed as follows:

$$\mathrm{NAR} = 8.17(\mathrm{NRI})^{0.9466} \quad (10)$$

The best-fit line is treated as the critical line (FS = 1), which separates the not-yet failed slopes (white dots) and the failed slopes (black dots) in a rainfall event. If the characteristic of a rainfall event falls above the line, then the slope is very likely to fail. If the characteristic of a rainfall event falls below the line, then the slope will remain stable or in the not-yet failed condition. In other words, if the NAR value is greater than that calculated from Eq. 10, it is very likely to lead to a slope failure.

Equation 10 not only provides information about landslide potential for a given rainfall event, but also can be used to estimate the critical time of landslide. By derivation of Eq. 10, the gradient of the best-fit line ($\Delta y/\Delta x$) in Fig. 9 is equal to the duration of rolling rainfall (ΔT) and can be expressed as

$$\Delta T = 7.734(\mathrm{NRI})^{-0.0534} \quad (11)$$

The unit of ΔT is in hour.

Recall the definition of ΔT illustrated in Fig. 9, $\Delta T = T_{\mathrm{f}} - T_{\mathrm{o}}$. If the starting time of rolling rainfall is known from the rainfall record, then, the critical time of landslide can be calculated by

$$T_{\mathrm{f}} = T_{\mathrm{o}} + 7.734(\mathrm{NRI})^{-0.0534} \quad (12)$$

Equation 11 is a power function equation. So, the duration time of rolling rainfall (ΔT) will decrease with increasing NRI. Using Eq. 11, the duration time of rolling rainfall (= critical time) corresponding to the occurrence of landslides on the T18 road can be estimated from Fig. 9. Considering the variation in input parameter, the distribution of data points started from NRI = 10^{-5} mm^{-1} and end at NRI = 10^{2} mm^{-1}. If one substitutes these numbers to Eq. 11, the duration time of intense rainfall ranges from 6 to 14 h. This result shows that large variations in input parameters tend to generate a wide range of failure times.

Application of the model

To verify the suitability of the proposed model, some landslides reported in the literature are chosen here as test cases for the proposed model. This step is necessary to evaluate the applicability of the proposed model to other slope cases.

Tenliao landslide, Taipei, Taiwan

A landslide on the Tenliao slope, Northern Taipei, occurred at 2:00 p.m. on November 1, 2000, when the strong typhoon Xangsane passed through northern Taiwan. Chen et al. (2005b) analyzed the development of transient pore water pressure on the landslide by the TRIGRS method. Using the GIS analysis, the landslide area was mapped into three categories: crest of slope, bare, and vegetated areas.

Following the data provided by Chen et al. (2005b), the factor of safety of the Tenliao slope during typhoon Xangsane is recalculated and shown in Fig. 10. At the crest

area of Tenliao slope, all the rainfall infiltrated into subsurface slope and the wetting front managed to reach up to 3.8 m in depth under the rainfall brought in by typhoon Xangsane. But, at the bare area, rainwater only partly infiltrated into the slope and the remaining rainfall became the run-off (Fig. 10a). In this bare area, the saturation zone reached up to 3.2 m in depth. For the vegetated area, a small amount of infiltrated rainwater was observed during Typhoon Xangsane as shown in Fig. 10a. In this area, the depth of the saturation zone was as low as 0.028 m (28 cm).

The results presented in Fig. 10 are able to explain the mechanism of the landslide at Tenliao slope during typhoon Xangsane. Slope instability was initiated at the crest area of Tenliao slope. A landslide is estimated to occur at after 11:00 a.m. Rainwater infiltration and rainwater run-off caused a landslide in the bare slope area at 2:00 p.m. Slope covered by vegetation remained stable during typhoon Xangsane. Combination of rain infiltration and water run-off caused debris flow after 2:00 p.m. This evidence is in agreement with the landslide mechanism reported by Chen et al. (2005b).

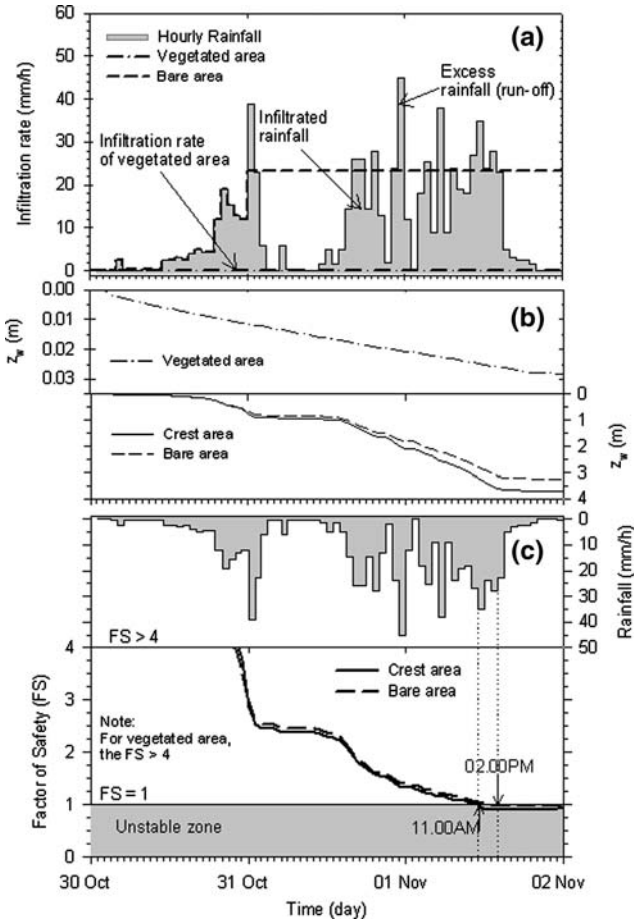

Fig. 10 Relationship between NRI and NAR for rainfall-induced landslides

Boso Peninsula landslide, Japan

Matsushi (2006) reported two landslide cases in the Boso Peninsula, Japan. In this area, two different slope sites were studied. One was in a sandstone area and the other was in a mudstones area. The depths of landslide in sandstone and mudstone area were measured at 1.4–1.7 m and 0.6–0.7 m, respectively. The infinite slope model was used to analyze the slope stability. Both the variations of monitored suction and water content during rainfall were considered in the analysis.

Figure 11 presents the results of rainfall infiltration, depth of wetting front, and safety factor of slope calculated from the proposed model. Figure 11a shows that rainfall infiltrates into the slope at the sandstone site. In contrast, rainfall at the mudstone slope was in excess of the rain infiltration process. The depth of rain infiltration reached 1.3 m below ground surface at the mudstone site and 1.8 m at the sandstone sites, respectively (Fig. 11b). Slope stability analysis shows that the mudstone slope probably slid 10 h (on August 1, 1989 at 5:11 a.m.) after the beginning of the rainstorm. In the case of the sandstone slope, the landslide was estimated to occur on August 1, 1989 at 8:24 a.m. It was about 14 h after the beginning of the rainstorm. The corresponding depth of wetting front at the time of landslide occurrence reached 0.5 m for mudstone site and 1.2 m for sandstone site, respectively (Fig. 11b). Matsushi and Matsukura (2007) estimated that landslides might occur at 4:00–6:00 a.m. on the mudstone slope and 7:00–10:00 a.m. on the sandstone slope. The occurrence time and depth of landslide, estimated from the proposed model is in agreement with that reported by Matsushi and Matsukura (2007).

Northern Tuscany landslide, Italy

Casagli et al. (2005) and Tofani et al. (2006) investigated landslide events in northern Tuscany area, Italy. During the November 20–21, 2001 rainstorm, several landslides occurred in Uzzano, Masa e Cozzile, and Colodi sites. These landslides, which were triggered by rainwater infiltration, were analyzed using SEEP/W and SLOPE/W. Slope instabilities occurred at 6:00 a.m. on November 21, 2000, at the Uzzano site and at 10:30 and 04:30 p.m. on November 20, 2000 for the Massa e Cozzile site and the Collodi site, respectively.

By inputting the information of slopes in Tuscany, Italy and the rainfall data to the proposed model, the variation of

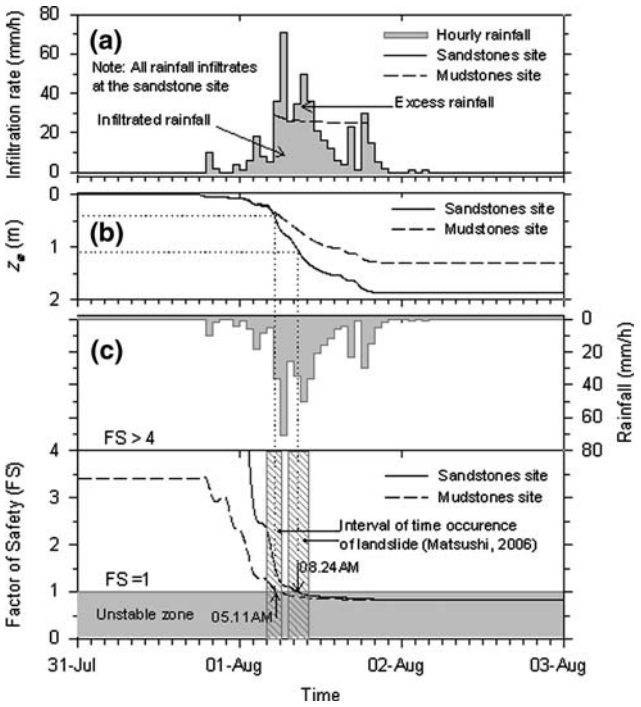

Fig. 11 **a** Infiltration rate, **b** Depth of wetting front, and **c** Variation in the factor of safety for mudstone and sandstone slopes

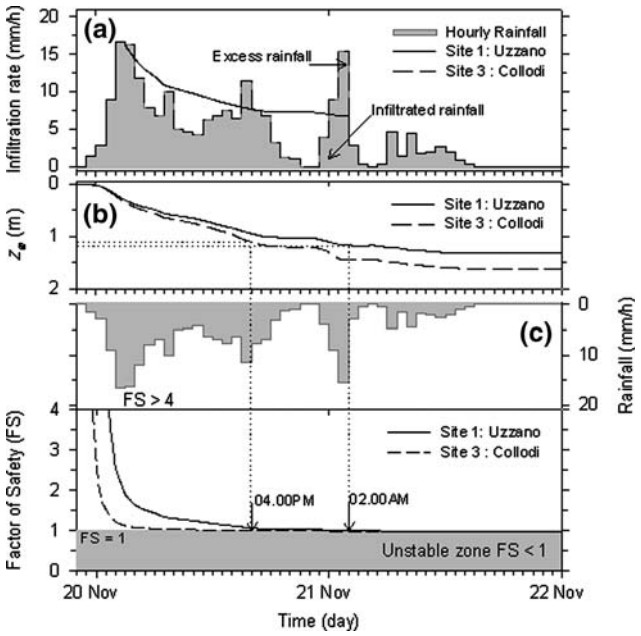

Fig. 12 **a** Infiltration rate, **b** Depth of wetting front, and **c** Variations in factor of safety at Uzzano and Colodi sites

safety factor is shown in Figs. 14 and 15. During the rainstorm, all the rainwater infiltrated into the slope at the Colodi site where the slope is covered by colluvial soil. The colluvial soil at the Colodi site has a higher permeability than at the other two sites (Fig. 12a). Rainwater runoff is expected to occur at Uzzano and Masa e Cozzile sites as shown in Figs. 12a and 13b. At the end of the rainstorm, the rainwater had infiltrated to a depth of 1.5–1.6 m for all sites studied (see Figs. 12b, 13b). At the occurrence time of landslides, the depth of wetting front reached 1.1–1.2 m below ground surface. This result is similar to the investigation done by Tofani et al. (2006). The depth of main scarp was found to be ranging from 1 to 1.5 m. The factor of safety calculated in Figs. 12c and 13c shows that slopes are prone to slide around 28 h (at 2:00 a.m. on November 21, 2000), 22 h (at 10:00 p.m. on November 20, 2000), and 18 h (at 4:00 p.m. on November 20, 2000) after the beginning of the rainstorm at the Uzzano, Masa e Cozzile, and Colodi sites, respectively. The calculated time of landslide is slightly different from the time predicted by Casagli et al. (2005) and Tofani et al. (2006). The difference mainly comes from the cohesion of soil used in this study. The cohesion was set to 0 by Casagli et al. (2005) and Tofani et al. (2006) in their analysis. But the cohesion of the soil is set to 8.8, 4.2, and 5.5 kPa for the Uzzano, Masa e Cozzile, and Collodi sites, respectively in this analysis.

Tung Chung East landslide, Hong Kong

Lan et al. (2003) investigated the rainfall-induced landslide in Tung Chung East, Lantau Island. The slope stability was analyzed according to the rainfall event on June 11, 2001. Three sites, with different geologic settings were analyzed using the TRIGRS method, namely: the completely deposited volcanic (CDV) rock, colluvial (Col), and residual soil (Res). The predicted results indicated that the CDV slope was stable with minimum factor of safety equal to 1.5. But, the colluvial and residual soil slopes might be prone to fail at about 8–11 h after the beginning of the rainstorm.

By inputting the information of slopes in Hong Kong and the rainfall data to the proposed model, the potential infiltration rate, variation of the wetting front depth and change of safety factor related to elapsed rainfall time are shown in Fig. 14. In Fig. 14a, all the rainwater infiltrates into the colluvial slope (SP8) due to the high permeability of this slope. But, in CDV (SP6) and residual soil (SP10) slopes, excess rainfall started about 4 and 10 h after the rainstorm began. The depth of wetting front extends to 1, 1.6, and 2.5 m from the ground surface in SP10, SP6, and SP8 slopes, respectively, as shown in Fig. 14b. Lan et al. (2005) recorded that the observed depth of wetting front in the slopes was up to 1.5–2.5 m from ground surface. The results of stability analysis shown in Fig. 14c indicate that CDV slope can remain stable with a minimum factor of safety = 1.45. But the other two slopes, colluvial and residual soil slopes showed tendencies toward failure 9 and

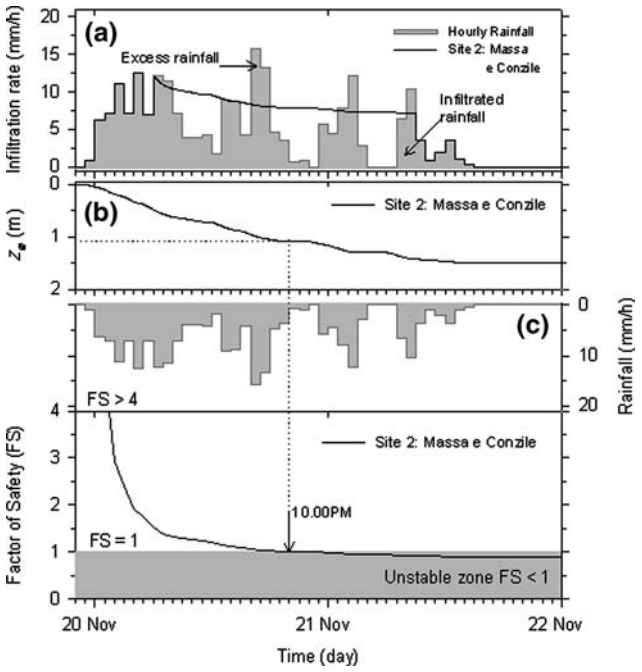

Fig. 13 **a** Infiltration rate, **b** Depth of wetting front, and **c** Variation in factor of safety at Masa e Cozzile site

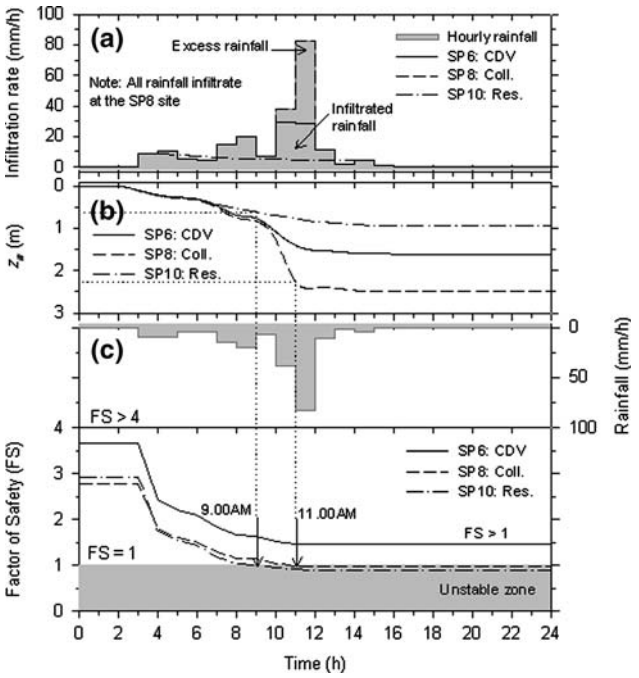

Fig. 14 **a** Rain infiltration, **b** Depth of wetting front, and **c** Slope stability vs. rainfall, Tung Chung East, Hong Kong

11 h, respectively, after the rainstorm began. These results are in good agreement with those reported by Lan et al. (2003). Table 3 summarizes the hydraulic and soil shear strength parameters obtained from the back-analysis on each landslide case.

Application of the proposed model to the landslide cases mentioned above has shown a good agreement in estimating the occurrence time of landslide. Use of the NAR and NRI in Eq. 9, Fig. 15 shows the data points of failed and not-yet failed slopes. Similar to Fig. 9, if the data points fall above the critical line (Eq. 10), then rainfall-induced landslides will happen. However, if the data points fall below the critical line, then landslides will not happen. From the data points in Fig. 15, it can be seen that some rainfall event, which results in no landslides may be above the critical line and some rainfall event leading to a failed slope may fall below the critical line. Using statistical and probability analyses, the rainfall events fall consistently on each zone (failed and not-yet failed zone) with probability $P(X) = 0.75$. This probability analysis indicates that the threshold rainfall Eq. 10 can be used to predict the potential for landslide occurrence when the probability reaches 0.75. It also implies that that the threshold rainfall shown in Fig. 11 can be used also to estimate the occurrence of landslide. Once the field collected or forecast rainfall data can be obtained from Weather Forecasting Organizations, then Eq. 10 can be used to predict the potential for landslide occurrence in any slope. By integrating all information needed, the proposed NAR–NRI relationship and Eq. 10 can be applied to establish a "landslide early-warning" system. However, it should be noted that this model is sensitive to input parameters such as suction head, cohesion, and internal friction angle. Therefore, a well-defined field and laboratory test should be performed in advance to yield a reasonable result.

Conclusions

Based on the study of the potential rain infiltration triggered shallow landslides, the following conclusions can be drawn:

1. Slopes with different permeabilities show different slope stability under the same rainfall conditions. Rainwater infiltrates to a deeper depth in slopes with higher permeability (k_{sat} = 36–360 mm/h) or to a shallower depth in slopes with lower permeability (k_{sat} = 0.36–3.6 mm/h). For rain infiltration induced slope failure, a slope tends to have a slip surface at a depth about 1.5–3.0 m below the surface.
2. If a slope failure is to occur, slopes with higher permeability tend to fail prior to the occurrence of maximum rainfall intensity. But for slope with lower permeability, it will need more intensive rainfall and a longer rain period before a slope failure happens. Based on the results generated from the proposed model, if a slope failure is to occur on a slope with lower permeability, it is very likely to fail subsequent to the occurrence of the maximum rainfall intensity.

Table 3 Hydraulic and soil shear strength parameters used to reanalyze different landslide cases

Landslide cases	β	k_{sat} (mm/h)	$\Delta\theta$	ψ_f (mm)	c' (kPa)	ϕ'	γt (kN/m^3)
Tenliao, Taiwan							
Crest area	50°	360	0.1	0.7	5	28°	19
Bare/uncovered area	50°	36	0.2	0.7	5	28°	19
Vegetated area	50°	0.036	0.1	0.7	10	32°	19
Boso Peninsula, Japan							
Sandstones site	40°	108	0.31	100	3.17	28.3°	17.3
Mudstones area	35°	28.8	0.33	50	1.01	27.7°	16.3
Tuscany, Italy							
Uzzano site	42.8°	3.96	0.2	840	8.8	32°	19.4
Masa e Cozzile site	16.1°	4.68	0.14	760	4.2	20°	18.7
Colodi site	36.5°	28.8	0.16	720	5.5	35°	19
Tung Chung East, Hong Kong							
CDV site	23.34°	27.36	0.1	152.9	2	28°[a]	19
Colluvium site	32.95°	540	0.1	50.9	2	30°[a]	19
Residual soil site	29.21°	3.6	0.1	305.9	2	23°[a]	19

[a] Irfan (1998)

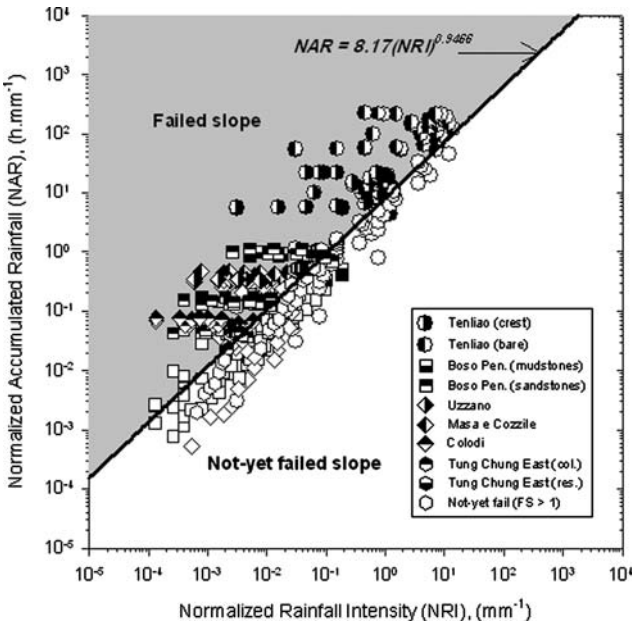

Fig. 15 Normalized accumulated rainfall–NRI relationship for the landslides collected from the literatures

3. The failure time of a slope depends on the rainfall parameters (intensity, duration, and accumulated rainfall) and the hydraulic and mechanical properties of the slope. The ability of the proposed model to predict the time of slope failure has been verified in this study. However, the method needs detailed information on the hydraulic and mechanical properties of a slope to generate realistic results. In general, the analytical method can be applied to slopes for which the hydrological, hydraulic, and geotechnical data are available.
4. To study threshold rainfall triggered slope failure, the NAR–NRI graph is also proposed in this paper. This graph can be used as a tool to predict the landslide potential of a slope and the occurrence time of the landslide. Using the NAR–NRI graph and Eq. 11, the time of the landslide on the T18 road was estimated to be from 6 to 14 h after the beginning of rolling rainfall. The applicability of the NAR–NRI relationship to landslides in different countries is also studied and the results are satisfactory.

References

Arya LM, Paris JF (1981) A physical-empirical model to predict the soil moisture characteristic from particle size distribution and bulk density data. Soil Sci Soc Am J 45:1023–1030

Casagli N, Dapporto D, Ibsen ML, Tofani V, Vannocci P (2005) Analysis of triggering mechanism during the storm of 20–21 November 2000 in northern Tuscany. Landslides 3(1):13–21

Chang M-S, Chiu Y-F, Lin S-Y, Ke T-C (2005) Preliminary study on the 2003 slope failure in Woo-Wan-Chai Area, Mt. Ali Road, Taiwan. Eng Geol 80:93–114

Chen C-Y, Chen T-C, Yu F-C, Yu W-H, Tseng C-C (2005a) Rainfall duration and debris-flow initiated studied for real-time monitoring. Environ Geol 47:715–724

Chen C-Y, Chen T-C, Yu W-H, Lin S-C (2005b) Analysis of time-varying rainfall infiltration induced landslide. Environ Geol 48:466–479

Chen L, Young MH (2006) Green-Ampt infiltration model for sloping surface. Water Resour Res 42:1–9. doi: 10.1029/2005WR104468

Chow V-T, Maidment DR, Mays LW (1988) Applied hydrology. McGraw-Hill, New York, pp 110-116; Ch. 4

Claunitzer V, Hopmans JW, Starr JL (1998) Parameter uncertainty analysis of common infiltration models. Soil Sci Soc Am J 62:1477–1487

Fredlund DG, Morgenstern NR, Widger RA (1978) The shear strength of unsaturated soils. Can Geotech J 15(3):313–321

Hsu S-M, Ni C-F, Hung P-F (2002) Assessment of three infiltration formulas based on model fitting on Richard's equation. J Hydrol Eng 7(5):373–379

Irfan TY (1998) Structurally controlled landslides in saprolitic soils in Hong Kong. Geotech Geol Eng 16(3):215–238

Lan H-X, Lee C-F, Zhou C-H, Martin CD (2005) Dynamic characteristics analysis of shallow landslides in response to rainfall event using GIS. Environ Geol 47:254–267

Lan H-X, Zhou C-H, Lee C-F, Wang S-J, Wu F-Q (2003) Rainfall-induced landslide stability analysis in response to transient pore pressure: a case study of natural terrain landslide in Hong Kong. Sci China E Technol Sci 46:52–68

Land Engineering Consultant Co. Ltd. (2005) Report on sliding area investigation at T18 road mileage 28K + 900 − 31K + 500. Ministry of Transportation and Communication of Taiwan (in Chinese)

Liao H-J, Ching J-Y, Lee W-F, Wei J (2006) Landslides along mountain roads in Taiwan. In: Tham L-G, Chau K-T (eds) Proceeding of the seminar on the state-of-the practice of geotechnical engineering in Taiwan and Hong Kong, 20 January 2006. Hong Kong, pp 75–99

Matsushi Y (2006) Triggering mechanism and rainfall thresholds for shallow landslides on soil-mantled hillslopes with permeable and impermeable bedrocks. Ph.D. dissertation, Graduate School of Life and Environmental Sciences, University of Tsukuba, Tsukuba, 109p

Matsushi Y, Matsukura Y (2007) Rainfall thresholds for shallow landsliding derived from pressure-head monitoring: cases with permeable and impermeable bedrocks in Boso Peninsula, Japan. Earth Surf Process Landforms 32:1308–1322

Muntohar AS, Liao H-J (2007) A prediction method for typhoon induced landslides along Alishan mountain road in Taiwan. Proceeding of the 4th international conference on disaster prevention and rehabilitation, Universitas Diponegoro, Semarang, 10–11 September 2007, pp 1–12

Rawls WJ, Ahuja LR, Brakensiek DL, Shirmohammadi A (1993) Infiltration and soil water movement. In: Maidment DR (ed) Handbook of hydrology. McGraw-Hill, New York; Ch. 5

Tofani V, Dapporto S, Vannocci P, Casagli N (2006) Infiltration, seepage and slope instability mechanisms during the 20–21 November 2000 rainstorm in Tuscany, central Italy. Nat Hazards Earth Syst Sci 6:1025–1033